Curved Density Fronts: Cyclogeostrophic Adjustment and Frontogenesis

CALLUM J. SHAKESPEARE

Research School of Earth Sciences, and ARC Centre of Excellence in Climate System Science, Australian National University, Canberra, Australian Capital Territory, Australia

(Manuscript received 8 June 2016, in final form 10 August 2016)

ABSTRACT

Curvature can play a significant role in the dynamics of density fronts at small scales and in low-latitude regions of the ocean. Fronts can be displaced from balance by rapid forcing and undergo an adjustment toward a more stable state or be strained and sharpened by surrounding flow in a process known as frontogenesis. This study investigates the role of curvature in adjustment and frontogenesis using the idealized configuration of an axisymmetric eddy and associated circular front. As a result of the curvature, the balanced state of this system is not geostrophic balance, where pressure and Coriolis forces exactly balance, but cyclogeostrophic balance, where pressure and Coriolis forces combine to supply a net inwards centripetal force on fluid parcels. The parameter range for which cyclogeostrophically balanced states exist for a given unbalanced initial condition is determined. This parameter range is smaller for anticyclonic fronts (i.e., fronts curved around a warm core), which have larger angular velocities than comparable straight fronts, implying they are more likely to break down during adjustment. The reverse is true for cyclonic fronts. A model for the sharpening of a curved front in a background strain flow, analogous to the Hoskins and Bretherton (1972) model for a straight front, is developed. Relative to a straight front subject to the same strain rate, vertical velocities are weaker for an anticyclonic front and stronger for a cyclonic front. Anticyclonic fronts collapse to a near discontinuity during frontogenesis far more rapidly than cyclonic fronts for the same strain rate.

1. Introduction

Regions of sharp horizontal density contrast, or fronts, are ubiquitous features near the ocean surface on scales from tens of meters to hundreds of kilometers (e.g., Shcherbina et al. 2013; Gula et al. 2014; Rosso et al. 2015; Capet et al. 2008; among others). These fronts are often generated on the periphery of eddies formed during the growth of barotropic and baroclinic instabilities (e.g., Holmes et al. 2014; Mahadevan 2006; Hoskins and Bretherton 1972). As such, many fronts are curved, with a radius of curvature comparable to the radius of the eddy. In some cases the eddy will remain in a stable, near-balanced state, while in other cases the curved front may be shed from the eddy and further strained and deformed by the surrounding flow field. The process by which an eddy and associated front attains a stable steady state is called adjustment, and the process by which a front is strained and sharpened is called frontogenesis. Adjustment and frontogenesis have previously been described theoretically for straight fronts by Blumen and Wu (1995) and Hoskins and Bretherton (1972), respectively. Here, we consider how these processes are modified when the front is strongly curved.

Curvature modifies the balanced state of the system from one of geostrophic balance, where pressure and Coriolis forces exactly balance, to one of cyclogeostrophic balance, where pressure and Coriolis forces combine to provide a net inwards centripetal force. Whether curvature is significant in a given eddy or front may be determined from the ratio of the centripetal acceleration v_θ^2/r to the Coriolis acceleration fv_θ or $C = v_\theta/(fr)$, where v_θ is the angular (alongfront) horizontal velocity, f is the Coriolis parameter, and r is the radius of curvature. We call C the cyclogeostrophy or cyclogeostrophic Rossby number. Curvature is important to the dynamics if C is nonnegligible. Examples include the tropics and highly energetic midlatitude regions such as the Gulf Stream, Kuroshio, and Antarctic Circumpolar Current. In the tropics, sharply curved fronts form on the northwestern edge (~6°N) of tropical instability vortices that have typical radii of 500 km and speeds of

Corresponding author address: Callum J. Shakespeare, Research School of Earth Sciences, Australian National University, 142 Mills Rd., Acton 2601, ACT, Australia.
E-mail: callum.shakespeare@anu.edu.au

DOI: 10.1175/JPO-D-16-0137.1

$1\,\mathrm{m\,s^{-1}}$, implying $C \sim 0.25$ (Flament et al. 1996; Holmes et al. 2014). In the Kuroshio, Niiler et al. (2003) found that curvature effects can modify speeds by up to 25% with respect to the geostrophic prediction (i.e., $C \sim 0.25$). Similar numbers ($C = 0.1$–0.3) have been reported in the Gulf Stream meanders (Liu and Rossby 1993). These examples emphasize the dynamical importance of curvature in many regions of the ocean.

Previous theoretical descriptions of fronts have examined the idealized configuration of a front that is infinitely long and straight, such that the solutions are essentially two-dimensional. Hoskins and Bretherton (1972), extending previous work by Eliassen (1962), Sawyer (1956), and Williams and Plotkin (1968), used this framework to formulate solutions for the nonlinear sharpening (so-called semigeostrophic frontogenesis) and ultimate collapse of a surface front as a result of straining by a larger-scale background flow. Their key result was that density fronts may sharpen to a near-discontinuous state and generate very large vertical velocities in a finite time proportional to the inverse strain rate. These results form the basis of our theoretical understanding of frontal dynamics (Thomas et al. 2008) and the importance of fronts to the vertical flux of heat and other tracers into the ocean interior (e.g., Ferrari 2011).

Blumen and Wu (1995) also considered the configuration of an infinitely long and straight front but focused on the problem of geostrophic adjustment. In this problem the front is initialized in an unbalanced state and adjusts (nonlinearly) via the radiation of waves into its geostrophically balanced state. This ''initial condition problem'' provides an idealized representation of the response of a front to a very rapid surface forcing or interior acceleration that near-instantaneously pushes it out of balance. Building on work by Rossby (1938), Ou (1984), and Tandon and Garrett (1994), Blumen and Wu (1995) determined the geostrophically balanced state and the amount of energy released as waves as a function of the initial conditions. They also showed that a balanced state only exists for certain initial conditions; for others, the front will break down during the adjustment process.

Both the Hoskins and Bretherton (1972) and Blumen and Wu (1995) models have the same three key ingredients: geostrophic balance, conservation of potential vorticity, and conservation of (generalized) absolute momentum, $M = e^{st}(fx + v)$, where s is the strain rate. As such, Shakespeare and Taylor (2013) were able to combine the two models into a unified theory of geostrophic adjustment and frontogenesis for a straight front. Here, we develop an analogous unified theory of cyclogeostrophic adjustment and frontogenesis for an axisymmetric curved front. In this case, the key ingredients are cyclogeostrophic balance, conservation of potential vorticity, and conservation of (generalized) absolute angular momentum.

The paper is set out as follows: In section 2, we introduce the Boussinesq equations in cylindrical coordinates and their simplification for the idealized configuration of an axisymmetric eddy and associated circular front. This configuration is the curved analog of the infinitely long straight front used in previous theories. In section 2b, we formulate an equation to determine the cyclogeostrophically balanced state for a given potential vorticity distribution and compare with the geostrophic limit. In section 2c, we add an appropriate background strain flow to describe the forced frontogenesis of a curved front and compare to the straight-front case. Last, in section 3, we comment on the usefulness and limitations of our theory in describing curved fronts in the ocean.

2. Theory

Here, we employ the f-plane, hydrostatic Boussinesq equations in cylindrical coordinates:

$$\frac{\partial v_r}{\partial t} + v_r\frac{\partial v_r}{\partial r} + \frac{v_\theta}{r}\frac{\partial v_r}{\partial \theta} - \frac{v_\theta^2}{r} + v_z\frac{\partial v_r}{\partial z} - fv_\theta = -\frac{1}{\rho_0}\frac{\partial p}{\partial r}, \tag{1a}$$

$$\frac{\partial v_\theta}{\partial t} + v_r\frac{\partial v_\theta}{\partial r} + \frac{v_\theta}{r}\frac{\partial v_\theta}{\partial \theta} + \frac{v_\theta v_r}{r} + v_z\frac{\partial v_\theta}{\partial z} + fv_r = -\frac{1}{\rho_0 r}\frac{\partial p}{\partial \theta}, \tag{1b}$$

$$0 = -\frac{1}{\rho_0}\frac{\partial p}{\partial z} + b, \tag{1c}$$

$$\frac{1}{r}\frac{\partial}{\partial r}(rv_r) + \frac{1}{r}\frac{\partial v_\theta}{\partial \theta} + \frac{\partial v_z}{\partial z} = 0, \quad \text{and} \tag{1d}$$

$$\frac{\partial b}{\partial t} + v_r\frac{\partial b}{\partial r} + \frac{v_\theta}{r}\frac{\partial b}{\partial \theta} + v_z\frac{\partial b}{\partial z} = 0, \tag{1e}$$

where r is the radial coordinate, z is the vertical coordinate, and θ is the azimuthal angle, with the subscript of v indicating a velocity in that coordinate direction. Parameter $b = g(\rho_0 - \rho)/\rho_0$ is the buoyancy, ρ_0 is the reference density, and p is the pressure. Classical theories of fronts (e.g., Hoskins and Bretherton 1972; Blumen and Wu 1995) assume that the front is infinitely long and straight or equivalently that the solution is independent of one Cartesian coordinate direction. Here, we make the analogous assumption for a curved front: we assume that the front is axisymmetric or equivalently that the solution is independent of the azimuthal angle θ. With this assumption, the Boussinesq equations [(1)] reduce to

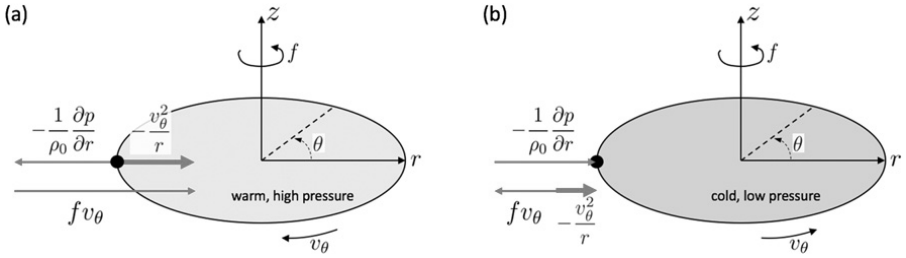

FIG. 1. Schematic of cyclogeostrophic balance for (a) anticyclonic fronts (warm-core eddies) and (b) cyclonic fronts (cold-core eddies). The pressure gradient and Coriolis accelerations acting on a fluid element (indicated by the black dot) traveling around the front are shown as thin red arrows, and the net centripetal acceleration is shown as a thick red arrow. The pressure gradient is assumed to have the same magnitude (but opposite direction) in (a) and (b). For anticyclonic fronts in (a) the Coriolis force must both balance the outward pressure gradient force and supply a net inward centripetal force, implying that the alongfront velocity v_θ must be relatively larger compared to geostrophic balance. For cyclonic fronts in (b), the pressure gradient supplies the inward centripetal force, resulting in a smaller Coriolis force and relatively lower velocities compared to geostrophic balance.

$$\frac{\partial v_r}{\partial t} + v_r\frac{\partial v_r}{\partial r} - \frac{v_\theta^2}{r} + v_z\frac{\partial v_r}{\partial z} - fv_\theta = -\frac{1}{\rho_0}\frac{\partial p}{\partial r}, \tag{2a}$$

$$\frac{\partial v_\theta}{\partial t} + v_r\frac{\partial v_\theta}{\partial r} + \frac{v_\theta v_r}{r} + v_z\frac{\partial v_r}{\partial z} + fv_r = 0, \tag{2b}$$

$$0 = -\frac{1}{\rho_0}\frac{\partial p}{\partial z} + b, \tag{2c}$$

$$\frac{1}{r}\frac{\partial}{\partial r}(rv_r) + \frac{\partial v_z}{\partial z} = 0, \quad \text{and} \tag{2d}$$

$$\frac{\partial b}{\partial t} + v_r\frac{\partial b}{\partial r} + v_z\frac{\partial b}{\partial z} = 0. \tag{2e}$$

It is readily shown that these equations [(2)] conserve potential vorticity (PV):

$$\frac{Dq}{Dt} = 0, \quad \text{where} \quad q = \left(f + \frac{\partial v_\theta}{\partial r} + \frac{v_\theta}{r}\right)\frac{\partial b}{\partial z} - \frac{\partial v_\theta}{\partial z}\frac{\partial b}{\partial r}, \tag{3}$$

and

$$\frac{D}{Dt} = \frac{\partial}{\partial t} + v_r\frac{\partial}{\partial r} + v_z\frac{\partial}{\partial z}, \tag{4}$$

is the axisymmetric material derivative. An extra term $\partial_z b v_\theta/r$ appears in the PV compared to the expression for a straight front ($r \to \infty$). The expression for conservation of PV [(3)] will prove crucial to our analysis below.

a. Cyclogeostrophic balance

As detailed in standard texts (e.g., Holton and Hakim 2013, their section 3.2.5), there exists an explicit steady solution to (2) for vanishing cross-frontal circulation, $v_r = v_z = 0$, where

$$-\frac{v_\theta^2}{r} = fv_\theta - \frac{1}{\rho_0}\frac{\partial p}{\partial r}, \quad \text{and} \tag{5a}$$

$$0 = -\frac{1}{\rho_0}\frac{\partial p}{\partial z} + b. \tag{5b}$$

Taking a vertical derivative of (5a) and substituting for the pressure gradient from hydrostatic balance (5b) yields a modified thermal wind equation,

$$\left(\frac{2v_\theta}{r} + f\right)\frac{\partial v_\theta}{\partial z} = \frac{\partial b}{\partial r}, \tag{6}$$

sometimes called gradient wind balance (Holton and Hakim 2013). The steady state described by the above equations [in particular (5a)] corresponds to a three-way force balance between centripetal, Coriolis, and pressure gradient forces known as cyclogeostrophic balance. The net centripetal force is required to maintain the circular structure of the flow, unlike the steady state of a straight front ($r \to \infty$) where the Coriolis and pressure forces exactly balance (i.e., geostrophic balance). The effect of curvature on alongfront velocities, relative to the straight front geostrophic limit, may be deduced directly from (5a) and depends primarily on the direction of the pressure gradient. Figure 1 displays a schematic of cyclogeostrophic balance for the two cases with oppositely directed radial pressure gradients. In Fig. 1a, the front is curved around a relatively warm patch of fluid (a warm-core eddy), resulting in flow in the opposite direction to the local rotation vector—that is, an anticyclonic front/eddy. In Fig. 1b the front is curved around a relatively cool patch of fluid (a cold-core eddy), resulting in flow in the same direction as the local rotation vector—that is, a cyclonic front/eddy. Assuming the pressure gradient has the same magnitude—but opposite sign—in Figs. 1a and 1b, the red arrows show the force balance on an element of fluid moving in the front.

In the anticyclonic case (Fig. 1a), the Coriolis force must both balance the outward pressure gradient (as for a straight front) and also supply a net inward centripetal force to maintain the circular flow. The velocity must therefore be larger than that predicted by geostrophic balance; that is, curvature of a front about a warm pool tends to increase velocities. In the cyclonic case (Fig. 1b), the inward pressure gradient supplies the centripetal force, and the Coriolis force makes up the difference. Consequently the velocity will be smaller than that predicted by geostrophic balance; that is, the curvature of a front about a cold pool tends to reduce velocities.

More generally, the importance of curvature may be quantified by the ratio of the centripetal and Coriolis terms in (5a):

$$C = \frac{v_\theta}{f r_0}, \tag{7}$$

where r_0 is the radius of curvature of the front of interest. We call C the cyclogeostrophy or cyclogeostrophic Rossby number. Values of C close to zero imply that the effects of curvature are negligible, and the system is close to the geostrophic limit, whereas larger magnitudes (e.g., low latitudes or strongly curved fronts) imply that the effect of curvature is significant, and alongfront velocities will be notably larger ($C < 0$) or smaller ($C > 0$) than the geostrophic limit.

b. Cyclogeostrophic adjustment

Here, we will derive the equation defining cyclogeostrophic balance for an arbitrary radial PV distribution and determine the existence (or nonexistence) of balanced states for a specific PV distribution. The effect of curvature will be quantified by direct comparison of the cyclogeostrophic adjustment of an axisymmetric eddy (and associated front) with the geostrophic adjustment of a straight front [as described by Blumen and Wu (1995)] with the same PV variation. The description of cyclogeostrophic balance for a specified PV will also lead naturally to a description of frontogenesis driven by a large-scale strain flow in section 2c, as described by Hoskins and Bretherton (1972) for straight fronts.

As noted in section 1, a crucial part of both the Blumen and Wu (1995) and Hoskins and Bretherton (1972) models is the fact that absolute momentum, $M = fx + v$, is conserved for an infinitely long straight front oriented along the y axis. We begin our analysis with the analogous result for axisymmetric eddies as defined by the simplified Boussinesq equations in (2). The angular momentum equation [(2b)] can be rearranged to obtain

$$\frac{DL}{Dt} = 0, \quad \text{where} \quad L = r v_\theta + \frac{f r^2}{2} \tag{8}$$

is the absolute angular momentum that is conserved following a fluid parcel. We now define a new conserved coordinate

$$R = \sqrt{\frac{2L}{f}} = \sqrt{r^2 + \frac{2 r v_\theta}{f}}, \tag{9}$$

which we call the angular momentum coordinate, analogous to the momentum coordinate ($X = M/f$) used in classical straight-front theory (Blumen and Wu 1995; Hoskins and Bretherton 1972). The spatial derivative transforms associated with a coordinate change from regular cylindrical coordinates (r, z, t) to angular momentum coordinates (R, $Z = z$, $T = t$ may be derived as

$$\frac{\partial}{\partial r} = \frac{\partial R}{\partial r}\frac{\partial}{\partial R} = \frac{r + \dfrac{v_\theta}{f}}{R - \dfrac{r}{f}\dfrac{\partial v_\theta}{\partial R}}\frac{\partial}{\partial R}, \quad \text{and} \tag{10a}$$

$$\frac{\partial}{\partial z} = \frac{\partial}{\partial Z} + \frac{\partial R}{\partial z}\frac{\partial}{\partial R} = \frac{\partial}{\partial Z} + \frac{\dfrac{r}{fR}\dfrac{\partial v_\theta}{\partial Z}}{1 - \dfrac{r}{Rf}\dfrac{\partial v_\theta}{\partial R}}\frac{\partial}{\partial R}, \tag{10b}$$

where

$$r(R, v_\theta) = -\frac{v_\theta}{f} + \sqrt{\left(\frac{v_\theta}{f}\right)^2 + R^2}, \tag{10c}$$

via rearrangement of (9). The inverse Jacobian of the coordinate transformation is [from (10a)]

$$J^{-1} = \frac{\partial r}{\partial R} = R\left(r + \frac{v_\theta}{f}\right)^{-1}\left(1 - \frac{r}{fR}\frac{\partial v_\theta}{\partial R}\right). \tag{11}$$

Physical solutions in momentum coordinates are those where the inverse Jacobian is everywhere positive.

To form our desired cyclogeostrophic balance equation, all that is required is to cast the PV [(3)] and thermal wind [(6)] equations in angular momentum coordinates using the above derivative transforms. The PV is transformed by first rewriting in terms of the absolute angular momentum L,

$$q = \frac{1}{r}\left(\frac{\partial L}{\partial r}\frac{\partial b}{\partial z} - \frac{\partial L}{\partial z}\frac{\partial b}{\partial r}\right), \tag{12}$$

and then substituting for the angular momentum coordinate $L = fR^2/2$ to obtain

$$q = \frac{fR}{r}\left(\frac{\partial R}{\partial r}\frac{\partial b}{\partial z} - \frac{\partial R}{\partial z}\frac{\partial b}{\partial r}\right), \tag{13}$$

followed by the derivative transforms (10):

$$\begin{aligned} q &= \frac{fR}{r}\left[\frac{\partial R}{\partial r}\left(\frac{\partial b}{\partial Z} + \frac{\partial b}{\partial R}\frac{\partial R}{\partial z}\right) - \frac{\partial R}{\partial z}\frac{\partial b}{\partial R}\frac{\partial R}{\partial r}\right] \\ &= \frac{fR}{r}\frac{\partial R}{\partial r}\frac{\partial b}{\partial Z} \\ &= \frac{fR}{r}\frac{r + \frac{\upsilon_\theta}{f}}{R - \frac{r}{f}\frac{\partial \upsilon_\theta}{\partial R}}\frac{\partial b}{\partial Z}. \end{aligned} \tag{14}$$

Similarly, the transformed thermal wind equation is

$$R\left(\frac{2\upsilon_\theta}{r} + f\right)\frac{\partial \upsilon_\theta}{\partial Z} = \left(r + \frac{\upsilon_\theta}{f}\right)\frac{\partial b}{\partial R}. \tag{15}$$

Combining (14) and (15) to eliminate the buoyancy b, we obtain an equation for $\upsilon_\theta(R, Z)$ that is second order in R and Z:

$$\begin{aligned} &\left\{\frac{\partial}{\partial Z}\left[\frac{R\left(\frac{2\upsilon_\theta}{r} + f\right)}{r + \frac{\upsilon_\theta}{f}}\frac{\partial}{\partial Z}\right] + \frac{\partial}{\partial R}\left[\frac{qr^2}{f^2 R\left(r + \frac{\upsilon_\theta}{f}\right)}\frac{\partial}{\partial R}\right]\right\}\upsilon_\theta \\ &\quad = \frac{\partial}{\partial R}\left[\frac{q}{f\left(1 + \frac{\upsilon_\theta}{rf}\right)}\right]. \end{aligned} \tag{16}$$

This nonlinear partial differential equation (PDE) may be solved numerically[1] via an iterative procedure, subject to appropriate boundary conditions that are described below. Equation (16) defines the exact, nonlinear, cyclogeostrophic balance solution for angular velocity υ_θ for an axisymmetric eddy with PV distribution $q(R, Z)$ on an f plane.

In the ''mass imbalance'' adjustment problem (e.g., Blumen and Wu 1995), a fluid is initialized in a motionless state with a specified buoyancy distribution. Here, we will consider the mathematically tractable special case of a fluid confined between rigid boundaries at the ocean surface $z = 0$ and at some depth $z = -H$ with buoyancy

$$b(R, Z) = b_0(R)\left(\frac{Z}{H} + 1\right), \tag{17}$$

such that $b = b_0(R)$ on the upper boundary and $b = 0$ on the lower boundary. Since the velocity is (initially) zero, the corresponding PV from (14) is

$$q = f\frac{\partial b}{\partial Z} = \frac{f b_0(R)}{H}, \tag{18}$$

a function of R only. This system is out of balance and once released will adjust toward a state of cyclogeostrophic balance. Since the PV is conserved and depends only on R, which is also conserved, the PV distribution $q(R)$ will remain constant during this process [this would not be true for a more general state $q(R, Z)$]. Consequently, the relevant cyclogeostrophically balanced state for this system is defined by (16). For balanced states that exist, the difference in total energy between the initial state and the (lower energy) balanced final state corresponds to the amount of energy lost to internal waves during the adjustment process. The nonexistence of a balanced state for given initial conditions (i.e., a vanishing inverse Jacobian) implies the breakdown of the eddy and associated front during the adjustment process. It is likely this breakdown will involve the formation of frontal (e.g., baroclinic) instabilities that break the angular symmetry of the system.

We now specify the relevant boundary conditions for solving (16), given the above PV distribution [(18)]. The assumption of rigid vertical boundaries is crucial since $\upsilon_z = 0$ on these surfaces, and hence

$$\frac{Db}{Dt} = \frac{\partial b}{\partial T} = 0 \tag{19}$$

in angular momentum coordinates, or equivalently $b = b(R)$ on the boundaries for all time. Thus, the thermal wind equation [(15)] implies that on the upper boundary, where $b = b_0(R)$, we require that

$$\left[R\left(\frac{2\upsilon_\theta}{r} + f\right)\right]\frac{\partial \upsilon_\theta}{\partial Z} - \left[\frac{1}{f}\frac{\partial b_0(R)}{\partial R}\right]\upsilon_\theta = r\frac{\partial}{\partial R}b_0(R) \quad \text{at} \quad z = 0. \tag{20}$$

Analogously, for the bottom zero buoyancy boundary we have that

$$\frac{\partial \upsilon_\theta}{\partial Z} = 0 \quad \text{at} \quad z = -H. \tag{21}$$

These two boundary conditions (20) and (21) do not fully constrain the nonlinear PDE (16) away from the front since $\partial_R b_0(R) \to 0$ there, and thus both boundary conditions are effectively Neumann in form (leading to an infinite number of solutions). To determine the

[1] It is readily shown that (16) is elliptic everywhere for $q/f > 0$.

required additional condition, we write down the expression for the buoyancy b as determined from the PV equation [(14)]:

$$b = \int_{-H}^{Z} \frac{q(R) r \left(R - \frac{r}{f} \frac{\partial v_\theta}{\partial R} \right)}{fR \left(r + \frac{v_\theta}{f} \right)} dZ'. \tag{22}$$

The buoyancy boundary condition at $z = -H$ (i.e., $b = 0$) has been imposed in (22). To satisfy the surface boundary condition $b(z = 0) = b_0(R)$, we require that

$$\int_{-H}^{0} \frac{q(R) r \left(R - \frac{r}{f} \frac{\partial v_\theta}{\partial R} \right)}{fR \left(r + \frac{v_\theta}{f} \right)} dZ = b_0(R). \tag{23}$$

Substituting $q(R)$ from (18) and simplifying yields the integral constraint

$$\int_{-H}^{0} \left(\frac{1}{r + \frac{v_\theta}{f}} \right) v_\theta + \left[\frac{r^2}{R \left(r + \frac{v_\theta}{f} \right)} \right] \frac{\partial v_\theta}{\partial R} dZ = 0, \tag{24}$$

which must apply for all time [since the PV distribution $q(R)$ is conserved]. For the lateral boundary conditions, we require that the velocity vanishes in the far field or

$$v_\theta(R \to \infty) = 0. \tag{25}$$

We also require a continuous and differentiable velocity field at the center of the eddy:

$$v_\theta = \frac{\partial v_\theta}{\partial R} = 0, \quad \text{as} \quad R \to 0. \tag{26}$$

Equation (16), together with constraint/boundary equations (20), (21), (24), (25), and (26), provides a complete description of the cyclogeostrophically balanced state for an eddy with the PV profile [(18)].

The numerical solution proceeds by making an initial guess for the velocity, $v_\theta^0 = 0$, to compute the nonlinear coefficients in the equations, then solving the resulting linear equations using finite differences to find a new estimate for the velocity v_θ^1. The average of the new and old estimates, $v_\theta = (v_\theta^i + v_\theta^{i-1})/2$, is used to compute the nonlinear coefficients (square bracketed terms) for the next iteration. This iterative procedure is continued until the solution converges to below a specified error $(v_\theta^i - v_\theta^{i-1})/\max(v_\theta^i) < 10^{-5}$, which takes $O(20)$ iterations for typical parameter values.

1) AN EXAMPLE OF CYCLOGEOSTROPHIC ADJUSTMENT

Cyclogeostrophic adjustment, as described above, is the process by which an eddy and its associated front adjusts from some unbalanced initial condition toward its cyclogeostrophically balanced state. Here, we will consider an initially motionless circular lens of fluid of depth H and linear interior stratification N_i^2 in a linearly stratified ambient N_o^2. Assuming a monotonic transition between the inside and outside stratifications, a generic functional form for the PV $q(R)$ associated with this system is

$$q(R) = f[N_i^2 + (N_o^2 - N_i^2)F(R)], \tag{27}$$

where $F(R)$ is a differentiable function that equals zero inside the eddy and one outside, with a transition width of w. Here, we choose

$$F(R) = \begin{cases} 0 & R < R_0 - \frac{w}{2} \\ \sin^2 \left[\frac{\pi}{2w} \left(R - R_0 + \frac{w}{2} \right) \right] & R_0 - \frac{w}{2} \le R \le R_0 + \frac{w}{2}, \\ 1 & R > R_0 + \frac{w}{2} \end{cases} \tag{28}$$

where we must have $w < 2R_0$. The cyclogeostrophically balanced state corresponding to this initial condition is defined by the equations derived in the previous section. The potential energy for the initial state can be computed as

$$E_P = -\rho_0 \int_0^\infty \int_{-H}^{0} bz \, dz 2\pi r \, dr. \tag{29}$$

In the final balanced state, some of this energy will have been converted to kinetic energy,

$$E_K = \int_0^\infty \int_{-H}^{0} \frac{\rho_0}{2} v_\theta^2 \, dz 2\pi r \, dr, \tag{30}$$

and some will remain as potential energy, with the residual $\Delta E = E_P^1 - (E_K^2 + E_P^2)$ having been radiated away as internal waves during the cyclogeostrophic adjustment process.

Figure 2 displays the initial and adjusted state for parameter values appropriate to a low-latitude eddy ($f = 10^{-5}\,\mathrm{s}^{-1}$; approximately 5°N) of radius $R_0 = 100\,\mathrm{km}$, height $H = 100\,\mathrm{m}$, and transition width $L = 100\,\mathrm{km}$, with the inside stratification $N_i^2 = 2 \times 10^{-4}\,\mathrm{s}^{-2}$ and outside stratification $N_o^2 = 1 \times 10^{-4}\,\mathrm{s}^{-2}$. The initial unbalanced state with no motion is shown in Fig. 2a. The adjusted state of cyclogeostrophic balance defined by (16) is shown in Fig. 2b. Relative to the initial state, the

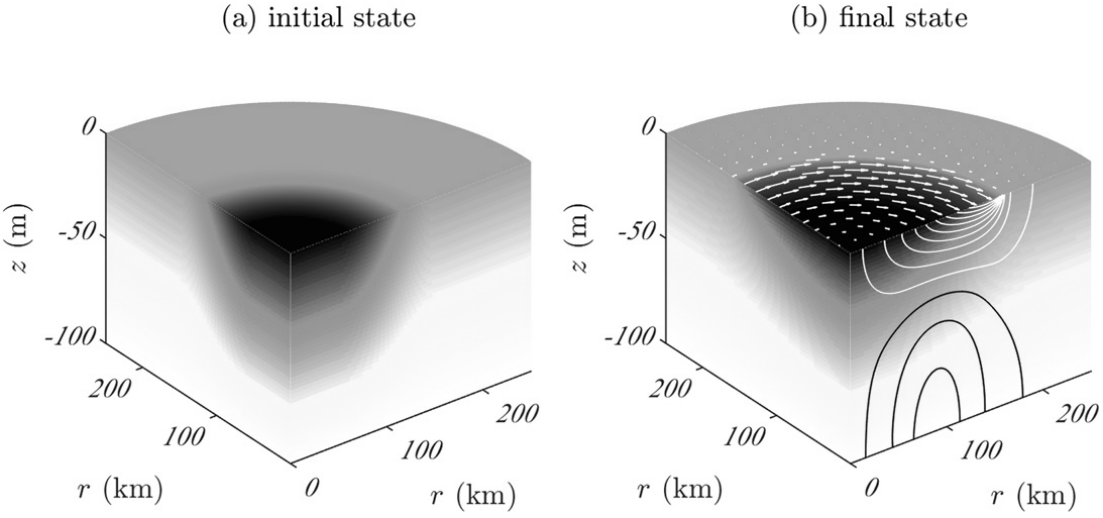

FIG. 2. The cyclogeostrophic adjustment of the circular lens of fluid with PV defined by (27) and parameter values: $f = 10^{-5}\,\mathrm{s}^{-1}$, $R_0 = 100\,\mathrm{km}$, $H = 100\,\mathrm{m}$, $w = 100\,\mathrm{km}$, $N_i^2 = 2 \times 10^{-4}\,\mathrm{s}^{-2}$, and $N_o^2 = 1 \times 10^{-4}\,\mathrm{s}^{-2}$. (a) The initial unbalanced state with no motion. (b) The final state of cyclogeostrophic balance. Colors indicate buoyancy, with darker colors denoting lighter fluid. The flow is indicated in (b) via vectors in the surface plane and contours of v_θ along the radial transect. White contours denote clockwise velocities, and black contours denote anticlockwise.

adjusted state corresponds to a broader and shallower eddy, with smoothed internal density gradients but intensified surface gradients on the edge of the eddy. The adjustment process can be visualized by comparing the two states. The warm lens in the initial state (Fig. 2a) will begin to slump outwards under the influence of gravity, increasing frontal gradients. The Coriolis force will deflect this outward flow into a clockwise rotation $v_\theta < 0$. The rotational flow will continue to increase until it is large enough for the Coriolis force to balance the pressure gradient and supply an inward centripetal force. In reality, the system will oscillate around this adjusted state for a period of time as it radiates energy via the generation of internal waves. In Fig. 2, the decrease in potential energy between the initial and final states is $E_P^1 - E_P^2 = 99.5$ PJ (assuming $\rho_0 = 1025\,\mathrm{kg\,m^{-3}}$), of which 38.2 PJ is converted to kinetic energy in the final state, while the remaining ~60% radiates away.

2) COMPARISON OF GEOSTROPHIC AND CYCLOGEOSTROPHIC SOLUTIONS

To explore the parameter space of the problem, and investigate the existence of cyclogeostrophically adjusted states, it is useful to first nondimensionalize the problem. We introduce the following scales:

$$Z' = \frac{Z}{H}, \quad q' = \frac{qH^2}{f^3 R_0^2}, \quad R' = \frac{R}{R_0}, \quad r' = \frac{r}{R_0},$$
$$b' = \frac{bH}{f^2 R_0^2}, \quad v'_\theta = \frac{v_\theta}{R_0 f}, \tag{31}$$

where primes denote nondimensional quantities. The nondimensional velocity v'_θ is equivalent to the cyclogeostrophy C defined previously. The nondimensional PDE and boundary conditions determining the nondimensional velocity v'_θ are given in the appendix [(A1), (A3)]. The simplified PDE and boundary conditions describing the geostrophic limit $R_0 \to \infty$ are also given therein [(A4), (A6)]. Both sets of equations depend only on the nondimensional PV profile $q'(R')$, which for an isolated front involves three independent parameters: the PV "inside" the curved front $q_i = fN_i^2$, the PV "outside" the front $q_o = fN_o^2$, and the transition width w.

Figure 3 shows the maximum magnitude of the nondimensional flow speed $|v|/(fR_0)$, computed from the (Fig. 3a) cyclogeostrophic and (Fig. 3b) geostrophic solutions. The PV outside the eddy is set to $q'_o = 1$, and the PV inside varied from 1% to 300% of this value; this PV ratio q_i/q_o is shown on the y axis in Fig. 3. The x axis displays the width of the front as a fraction of the eddy radius w/R_0 and is varied from 0.1 to 1.9. The weakest fronts occur when the inside and outside PV is nearly equal or $q_o/q_i \to 1$. Black lines on the figure show parameter values for which the solution becomes discontinuous [i.e., the inverse Jacobian [(11)] and (A5) vanishes somewhere in the domain] as the PV difference is increased; continuous adjusted states exist only in the region including $q_o/q_i = 1$ between these lines. The ratio of maximum speeds in the two solutions is shown in Fig. 3c. Speeds in the cyclogeostrophic solution are greater from warm eddies (up to ~30%) and lesser (up to ~20%) for cold eddies, relative to the geostrophic

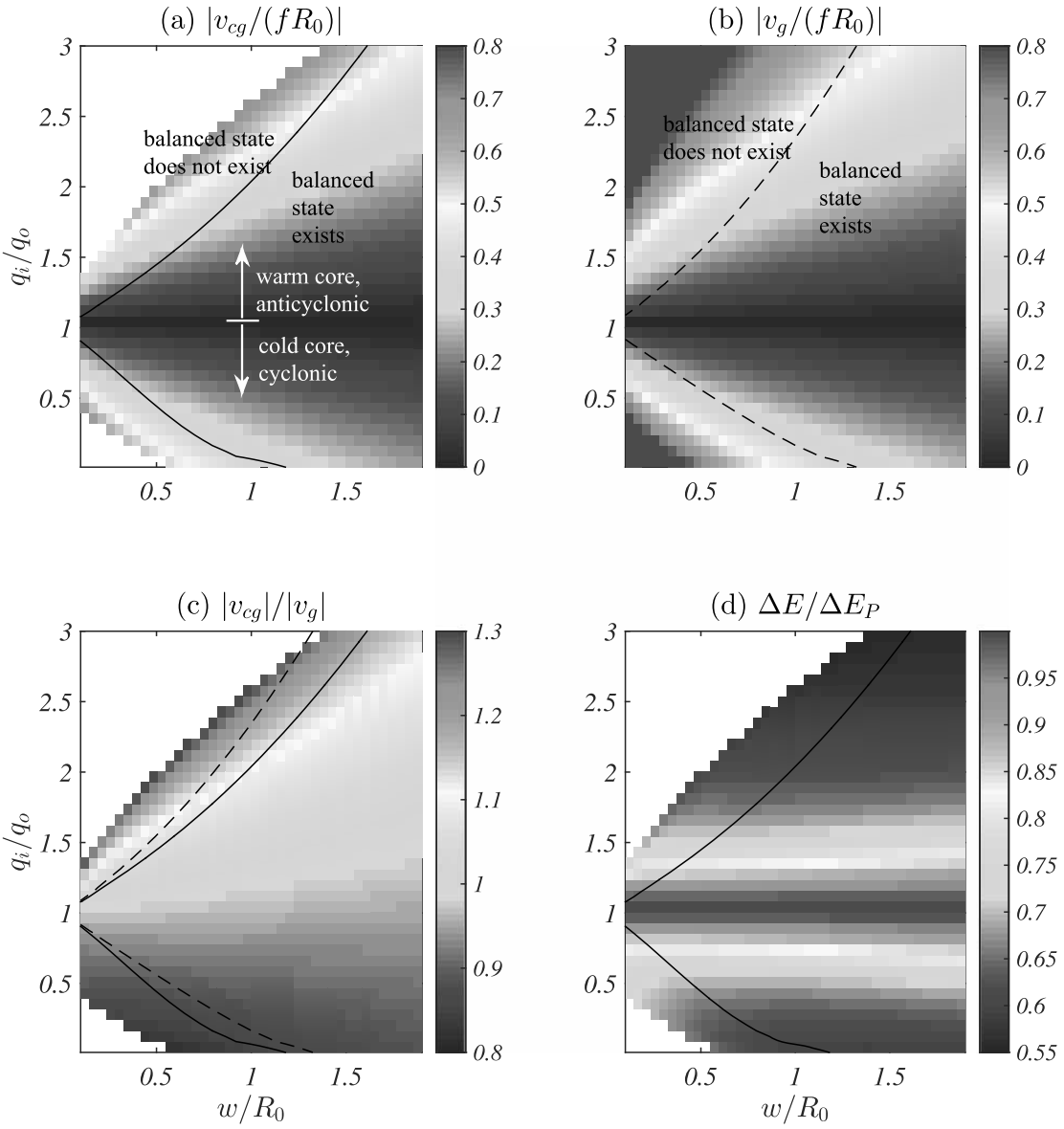

FIG. 3. The maximum speeds in the (a) cyclogeostrophic and (b) geostrophic balance solutions for a specified PV distribution in (27). Here, $q_o' = 1$, and the maximum velocities are compared for a range of frontal widths w/R_0 and PV ratios q_i/q_o. (c) The ratio of the maximum velocities v_{cg}/v_g. (d) The fraction of the change in potential energy radiated away (rather than converted to kinetic energy) when an initially motionless lens of fluid adjusts to its cyclogeostrophically balanced state. The black lines denote the parameter values for which the steady state becomes discontinuous in the cyclogeostrophic (solid) and geostrophic (dashed) solutions. White regions are where the numerical solution did not converge.

solution. Correspondingly, discontinuities form for smaller PV contrasts and larger transition widths for warm eddies, relative to the geostrophic solution. The reverse is true for cold eddies.

Figure 3d shows the fraction of energy radiated during cyclogeostrophic adjustment. Specifically, $\Delta E/\Delta E_p$ is the net difference in energy, $\Delta E = E_P^1 - E_P^2 - E_K^2$, normalized by the difference in potential energy, $\Delta E_P = E_P^1 - E_P^2$, between an initial motionless state (e.g., Fig. 2a) with the specified PV distribution $q(R)$ and the state of cyclogeostrophic balance (e.g., Fig. 2b). The fraction is largest (close to 1) for eddies/fronts with small PV contrasts and decreases for large PV contrasts.

c. Cyclogeostrophic frontogenesis

In this section, we will extend our model of cyclogeostrophic balance [(16)] to describe time-dependent forced frontogenesis. The Hoskins and Bretherton (1972) model describes how a (straight) front is sharpened by the action of a background strain flow. The

strain flow perturbs the cross-frontal geostrophic balance, generating a ''secondary circulation'' around the front to restore balance. The question to be addressed here is how curvature modifies these dynamics: specifically, how does the secondary circulation and associated vertical velocities change when curvature is considered?

First, we need to introduce an appropriate horizontal background flow that drives straining across the front (in the radial direction).[2] There is only one possible form for a purely horizontal flow that is both independent of θ and volume conserving:

$$\overline{v}_r = \frac{a(t)}{r} \tag{32}$$

for some time-dependent function $a(t)$. This flow corresponds to a uniform radial volume flux of $2\pi r\overline{v}_r = 2\pi a(t)$ per unit height throughout the domain and therefore implies a point source of volume at $r = 0$. In practice, this behavior suggests that solutions will only be physically meaningful sufficiently far away from $r = 0$. The confluent radial strain rate associated with (32) is

$$-\frac{\partial \overline{v}_r}{\partial r} = \frac{a(t)}{r^2}. \tag{33}$$

Consider the effect of this flow on a front of width Δr initially centered at $\mathscr{R} = R_0 \gg \Delta r$. The flow will (i) strain this front and reduce the width Δr and (ii) advect this front outwards, increasing the radius $\mathscr{R}$. Specifically, the radius $\mathscr{R}$ will evolve as

$$\frac{d\mathscr{R}}{dt} = \overline{v}_r|_{r=\mathscr{R}} = \frac{a(t)}{\mathscr{R}} \Rightarrow \mathscr{R}(t) = \sqrt{R_0^2 + 2\int_0^t a(t')\,dt'}. \tag{34}$$

Suppose we choose the function $a(t)$ to have the form

$$a(t) = sR_0^2 e^{2st} \tag{35}$$

for some constant $s > 0$. Then, it is easily shown that the location of the front defined by (34) evolves as $\mathscr{R}(t) = R_0 e^{st}$ and thus that the confluent strain rate at the location of the front is $a(t)/\mathscr{R}(t)^2 = s$ for all time. Since the strain rate at the front is constant with time, we have a direct analog to the Hoskins and Bretherton (1972) model where the strain rate is constant everywhere (including at the front). For this purely radial background flow field, the primitive equations [(1)] reduce to

$$f\overline{v}_r = -\frac{1}{\rho_0 r}\frac{\partial \overline{p}}{\partial \theta}, \quad \text{and} \tag{36}$$

$$\frac{\partial \overline{v}_r}{\partial t} + \overline{v}_r\frac{\partial \overline{v}_r}{\partial r} = -\frac{1}{\rho_0}\frac{\partial \overline{p}}{\partial r}, \tag{37}$$

which may be solved to obtain the background pressure field

$$\overline{p}/\rho_0 = -\frac{\overline{v}_r^2}{2} - 2s^2R_0^2e^{2st}\ln(r) - fsR_0^2e^{2st}\theta. \tag{38}$$

The background pressure field is discontinuous along a radial branch cut at some angle θ. The discontinuity is not a physical problem if we focus only on a small segment of curved front located sufficiently far from $r = 0$.[3] The equations for the perturbation flow are obtained by substituting $v_r = \overline{v}_r + v_r'$, $p = \overline{p} + p'$, and so on, into the primitive equations [(1)] and simplifying, assuming the perturbation fields (v_r', p', etc.) are independent of θ. Dropping the primes from the perturbation fields, the equations for the perturbation flow are

$$\frac{Dv_r}{Dt} - \frac{v_\theta^2}{r} - fv_\theta + \underline{v_r\frac{\partial \overline{v}_r}{\partial r}} = -\frac{1}{\rho_0}\frac{\partial p}{\partial r}, \tag{39a}$$

$$\frac{Dv_\theta}{Dt} + \frac{v_\theta v_r}{r} + fv_r + \underline{\frac{v_\theta \overline{v}_r}{r}} = 0, \tag{39b}$$

$$0 = -\frac{1}{\rho_0}\frac{\partial p}{\partial z} + b, \tag{39c}$$

$$\frac{1}{r}\frac{\partial}{\partial r}(rv_r) + \frac{\partial v_z}{\partial z} = 0, \quad \text{and} \tag{39d}$$

$$\frac{Db}{Dt} = 0, \tag{39e}$$

where

$$\frac{D}{Dt} = \frac{\partial}{\partial t} + \left(v_r + \underline{\overline{v}_r}\right)\frac{\partial}{\partial r} + v_z\frac{\partial}{\partial z}. \tag{39f}$$

The underlined terms in (39) are the new terms relative to the regular axisymmetric Boussinesq equations [(2)] that arise due to the background flow field. PV conservation [(3)] is unaffected by the background flow field (except for the change to the material derivative).

A key feature of the Hoskins and Bretherton (1972) model for strained straight fronts is that geostrophic

[2] In the straight front case, a flow of the form $\overline{u} = -sx$ and $\overline{v} = sy$ is employed, where $s = -\partial_x\overline{u}$ is the confluent strain rate.

[3] In general, we could add an arbitrary spatially uniform velocity to the background flow, for example, $\overline{v} = -sR_0e^{2st}\hat{\mathbf{x}}$, such that the velocity at a particular point on the front (in this case, $R = R_0$ and $\theta = 0$) will be zero for all time. This uniform background velocity will have no dynamical effect on the front but will cause the front to remain fixed in space rather than advecting outward. However, the radius of curvature will still increase.

balance holds across the front as long as the strain rate s is sufficiently small, $(s/f)^2 \ll 1$. We now derive the analogous result for curved fronts in a strain flow: that is, cyclogeostrophic balance holds across the front if the strain rate is sufficiently small. Referring to (39a), for cyclogeostrophic balance to hold across the front, we require

$$\frac{Dv_r}{Dt} \sim v_r \frac{\partial \overline{v}_r}{\partial r} \ll f v_\theta \sim \frac{v_\theta^2}{r} \sim \frac{1}{\rho_0}\frac{\partial p}{\partial r}. \tag{40}$$

The strain at the front is constant and equal to s, that is, $\partial_r \overline{v}_r = s$ at the front. Thus, we require that

$$v_r s \ll f v_\theta. \tag{41}$$

From the angular momentum equation [(39b)], we can write an expression for the radial perturbation flow:

$$v_r = -\frac{\dfrac{\partial v_\theta}{\partial t} + \overline{v}_r \dfrac{\partial v_\theta}{\partial r} + v_z \dfrac{\partial v_\theta}{\partial z} + \dfrac{v_\theta \overline{v}_r}{r}}{\dfrac{\partial v_\theta}{\partial r} + \dfrac{v_\theta}{r} + f}. \tag{42}$$

Since we are primarily interested in fronts located well away from $r = 0$ (the discontinuity in the background flow field), we anticipate that $\Delta r \ll r$ in regions of interest, and thus the smallest terms in the denominator in (42) are $f \sim v_\theta/r$. The largest terms in the numerator scale as $\overline{v}_r \partial_r v_\theta \sim \overline{v}_r/\Delta r v_\theta \sim s v_\theta$, and thus an upper limit on v_r is

$$v_r \sim \frac{s}{f} v_\theta. \tag{43}$$

Substituting this result (43) into (41), we have the requirement that for cyclogeostrophic balance to hold, the strain rate s must be small compared with f or

$$\left(\frac{s}{f}\right)^2 \ll 1. \tag{44}$$

However, similar to classical straight-front theory (e.g., Hoskins and Bretherton 1972), cyclogeostrophic balance (and thus our model) will break down as the front approaches a discontinuity.

Since the PV is unchanged by the addition of the background flow and cyclogeostrophic balance holds for sufficiently small strain rates, the model equation [(16)] derived in the previous section from these two constraints still applies at any given instant in time. All that remains in formulating a frontogenesis model is to determine how the PV q in (16) evolves with time in the strain flow. The angular momentum equation [(39b)] in the background flow field may be expressed as

$$\frac{DL}{Dt} = \frac{f}{2}\frac{DR^2}{Dt} = f\overline{v}_r r = sfR_0^2 e^{2st}, \tag{45}$$

where the total angular momentum L and angular momentum coordinate R are defined previously as (8) and (9). Equation (45) may be rewritten as

$$\frac{D\hat{R}}{Dt} = 0, \quad \text{where} \quad \hat{R}^2 = R^2 - R_0^2 e^{2st} + R_m^2, \tag{46}$$

and R_m is a constant and exceeds $R_0 e^{st}$ for times t of interest (this ensures $\hat{R}^2 > 0$ for all times of interest). Now suppose we have a PV distribution $q = q(\hat{R})$ at some time $t = \ln(R_m/R_0)/s$, such that $R = \hat{R}$. Since $\hat{R}$ is conserved and q is conserved, the PV distribution $q(\hat{R})$ is conserved, and the PV at any time will be

$$q = q(\hat{R}) = q\left(\sqrt{R^2 - R_0^2 e^{2st} + R_m^2}\right). \tag{47}$$

Substituting this expression for q into the model PDE [(16)] and the boundary conditions [(20)] completely describes the time evolution of a curved front in the background strain flow.

1) AN EXAMPLE OF CYCLOGEOSTROPHIC FRONTOGENESIS

The above equations use some large time $t = \ln(R_m/R_0)/s$ as a Lagrangian reference point to define the PV distribution; that is, $\hat{R} = R$ and $q(\hat{R}) = q(R)$ at this time.[4] Here, we choose an error function PV distribution of

$$q(\hat{R}) = \frac{f}{2}\left[1 + \operatorname{erf}\left(\frac{\hat{R} - R_m}{\dfrac{R_0 w}{R_m}}\right)\right](N_o^2 - N_i^2) + fN_i^2. \tag{48}$$

Substituting for $\hat{R}$ [(46)] and assuming that $R_0 \ll R_m$ and $|R - R_0| \ll R_0$, the corresponding PV at time zero is

$$q(R)|_{t=0} \simeq \frac{f}{2}\left[1 + \operatorname{erf}\left(\frac{R - R_0}{w}\right)\right](N_o^2 - N_i^2) + fN_i^2. \tag{49}$$

The cyclogeostrophic frontogenesis solution for a 30° segment of curved front is visualized in Fig. 4 for a particular set of parameter values. The front is initially

[4] It is necessary to use a large time rather than time zero as a reference point because the background flow field is continually adding new fluid (a volume flux of $r\overline{v}_r$ per radian) at the origin. This fluid only exists at large time, so to set its properties (PV) a large time must be used as the reference.

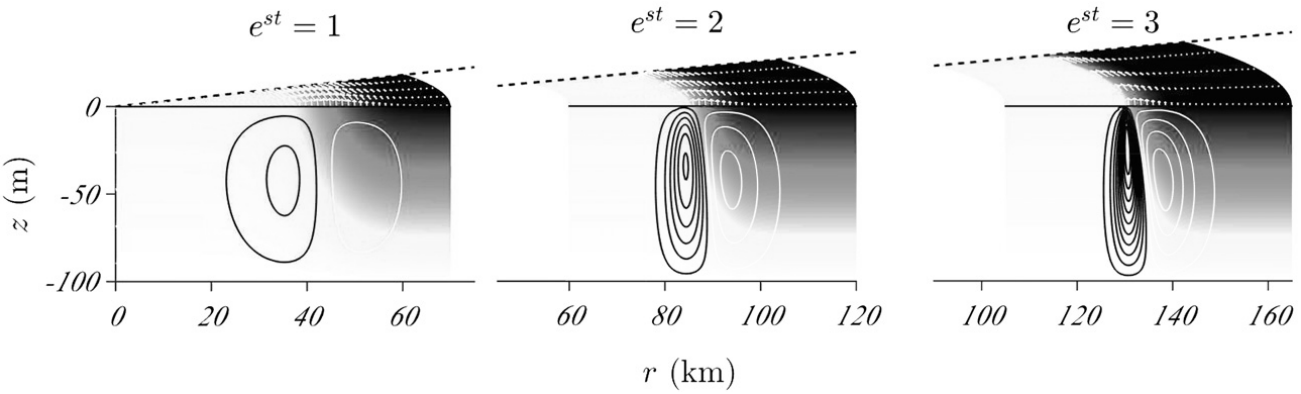

FIG. 4. The cyclogeostrophic frontogenesis solution for a 30° segment of curved front in a radial strain flow with parameter values: $f = 2 \times 10^{-5}\,\mathrm{s}^{-1}$, $R_0 = 45\,\mathrm{km}$, $H = 100\,\mathrm{m}$, $w = 10\,\mathrm{km}$, $N_i^2 = 2 \times 10^{-6}\,\mathrm{s}^{-2}$, and $N_o^2 = 2 \times 10^{-5}\,\mathrm{s}^{-2}$. An error function PV profile [(48)] is assumed. Colors indicate buoyancy with darker colors denoting higher buoyancy. Surface flow is represented using white vectors. Contours of vertical velocity are shown along the radial transect with black denoting negative velocities and white denoting positive velocities. The contour interval is $1\,\mathrm{m\,day}^{-1}$, assuming a strain magnitude of $s = 0.1f$ (the vertical velocity scales linearly with strain). The front is initially located at $R_0 = 45\,\mathrm{km}$ and has a transition width $w = 10\,\mathrm{km}$ at time zero ($e^{st} = 1$). As time increases, the front is advected outwards to location $R = R_0 e^{st}$ and the width decreases proportionately, amplifying the secondary circulation.

of PV transition width $w = 10\,\mathrm{km}$ and located at a radius of $R_0 = 45\,\mathrm{km}$. The solution is shown at times $t = 0, \ln(2)/s$, $\ln(3)/s$; the front moves outwards, its arc length increases, and it sharpens with time. The background strain flow drives a thermally direct secondary circulation, represented in the figure by contours of vertical velocity. The vertical velocity at any instant in time may be determined from buoyancy conservation [(39e)] in R coordinates:

$$0 = \frac{Db}{Dt} = \frac{DT}{Dt}\frac{\partial b}{\partial T} + \frac{DR}{Dt}\frac{\partial b}{\partial R} + \frac{DZ}{Dt}\frac{\partial b}{\partial Z} = \frac{\partial b}{\partial T} + \frac{sR_0^2 e^{2st}}{R}\frac{\partial b}{\partial R} + v_z\frac{\partial b}{\partial Z}, \tag{50}$$

where the material derivative of R is substituted from (45). Rearranging (50) yields the required expression

$$v_z = -\left(\frac{\partial b}{\partial T} + \frac{sR_0^2 e^{2st}}{R}\frac{\partial b}{\partial R}\right)\left(\frac{\partial b}{\partial Z}\right)^{-1}. \tag{51}$$

Time derivatives are computed numerically by solving the model PDE (16) at $T = t \pm \Delta t/2$ and using finite difference formulae. The vertical velocity in the present example increases by an order of magnitude as the front sharpens.

2) COMPARISON OF GEOSTROPHIC AND CYCLOGEOSTROPHIC SOLUTIONS

The geostrophic, strain-forced frontogenesis solution is readily recovered from the cyclogeostrophic solution. The PDE for the geostrophic limit (A4) still applies—all that remains is to determine the time evolution of the momentum coordinate X in this equation. Taking the geostrophic limit [$v/(fR_0) \to 0$, $R_0 \to \infty$] of the conserved quantity $\hat{R}$ [(46)] derived above yields

$$\frac{D\hat{X}}{Dt} = 0, \quad \text{where} \quad \hat{X} = e^{st}\left(x + \frac{v}{f}\right) = e^{st}X, \tag{52}$$

and $x = r - R_0 e^{st}$.[5] Thus, the geostrophic limit is described by the PDE (A4) with the PV as a function of time $q(\hat{X}) = q(Xe^{st})$; this is precisely the Hoskins and Bretherton (1972) model for the time evolution of an infinitely long straight front in a strain flow [here derived for a variable PV rather than the uniform PV assumed by Hoskins and Bretherton (1972)]. For comparison between the geostrophic and cyclogeostrophic models, we set the geostrophic model PV distribution such that the PV in the two models agrees at time zero or

$$q(\hat{X}) = \frac{f}{2}\left[1 + \mathrm{erf}\left(\frac{\hat{X}}{w}\right)\right](N_o^2 - N_i^2) + fN_i^2. \tag{53}$$

Since the alongfront velocity and buoyancy fields are uniquely determined from the cyclogeostrophic balance and PV conservation equations for a given PV, these fields will not match between different solutions at time zero. However, these initial differences are entirely a result of the curvature terms in the balance equations and are thus physically significant.

Figure 5 displays the time-dependent frontogenesis solutions for a particular set of parameter values

[5] The $\hat{X}$ is the "generalized momentum coordinate" introduced by Shakespeare and Taylor (2013). By analogy, $\hat{R}$ would be the "generalized angular momentum coordinate."

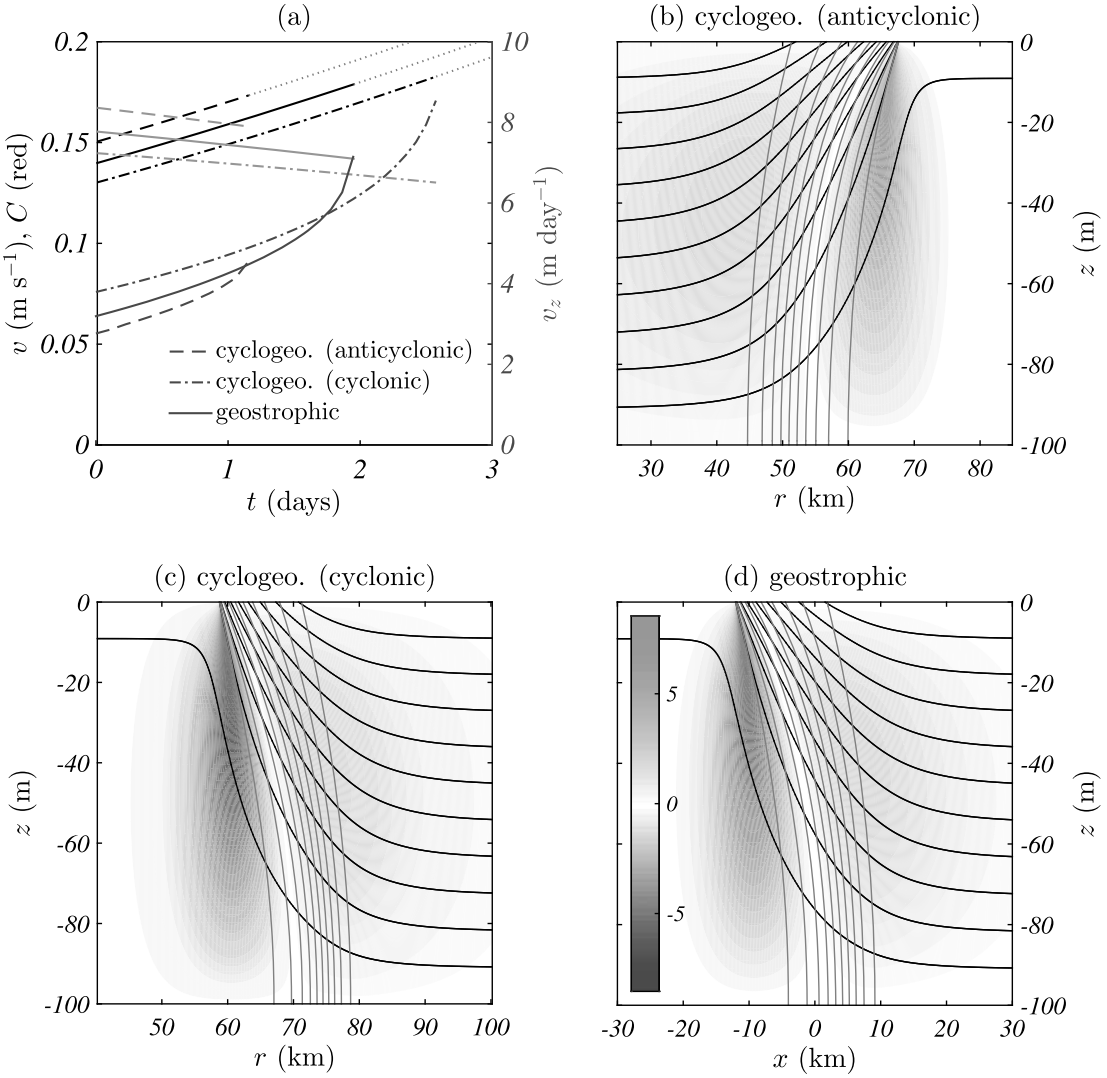

FIG. 5. Comparison of time-dependent frontogenesis solutions for parameter values $f = 2 \times 10^{-5}\,\mathrm{s}^{-1}$, $R_0 = 45$ km, $H = 100$ m, $w = 10$ km, $N_{ilo}^2 = 2 \times 10^{-6}\,\mathrm{s}^{-2}$, and $2 \times 10^{-5}\,\mathrm{s}^{-2}$. An error function PV profile is used: see (49) and (53). (a) Time series of the maximum magnitudes of the alongfront velocity v (black; m s^{-1}) and vertical velocity v_z (blue; m day^{-1}), assuming a strain of $s = 0.1f$, from the anticyclonic (dashed), cyclonic (dashed–dotted), and geostrophic (solid) solutions. The cyclogeostrophy of the front as a function of time, $C = |v|/(fR_0e^{st})$, is also shown in red. The vertical velocity (color; m day^{-1}), buoyancy (black contours), and PV (gray contours) just prior to the formation of a discontinuity in each solution is shown: (b) anticyclonic, (c) cyclonic, and (d) geostrophic.

corresponding to an initial cyclogeostrophy of $C = v/(fR_0) \simeq 0.15$ (see figure caption for parameter values). Three solutions are shown: the cyclogeostrophic in both cyclonic (cold core) and anticyclonic (warm core) configurations and the geostrophic. Figure 5a shows the time series of the maximum magnitudes of the alongfront velocity (v; black, left axis) and the vertical velocity (v_z; blue, right axis) from time zero up to the time at which each model manifests a discontinuity [$J^{-1} = 0$; cyclogeostrophic in (11); geostrophic in (A5)]. The vertical velocity (color, m day^{-1}), buoyancy (black contours), and PV (gray contours) are displayed just prior to the time of discontinuity formation for each solution in Figs. 5b, 5c, and 5d. The cyclogeostrophy of the front as a function of time, $C = |v|/(fr) = |v|/(fR_0e^{st})$, is also shown in red on Fig. 5a and decreases marginally with time due to the outward advection of the front by the strain flow. Since the cyclogeostrophy changes only marginally, curvature remains a significant effect over the time evolution of the front. As anticipated from previous results (e.g., Fig. 3), the maximum alongfront flow speeds at any given time are smallest for the cyclonic solution and largest for the anticyclonic, with the geostrophic in between (the differences are of the order of 10%). Reduced flow speeds are associated with a smoother surface front at a given time and thus an increased time for the formation of a discontinuity.

Discontinuities form when the velocity reaches $\sim 0.175\,\mathrm{m\,s^{-1}}$ for these parameters, which occurs at times $t = 1.2$, 2.6, and 1.9 days for the anticyclonic, cyclonic, and geostrophic solutions, respectively. Thus, curvature can lead to very significant ($\sim \pm 40\%$ in this case) changes in the time taken for frontal collapse.

Interestingly, the vertical velocities also differ significantly (15%), even at time zero. At time zero, the strongest vertical velocity occurs for the cyclonic solution, which has the weakest alongfront velocity and smallest frontal buoyancy gradient. The weakest vertical velocity occurs for the anticyclonic solution, which has the strongest alongfront velocity and largest frontal buoyancy gradient. This behavior is a result of the nonlinear slumping of the surface front into a background flow with a radially varying strain; at first order $r = R - v/f$, implying that the maximum PV/buoyancy gradient is shifted by $\Delta r = r - R = -v/f$ from where it is defined in momentum coordinates ($R = R_0$). The cyclonic front slumps radially inward and thus the background strain at the location of the front is larger: at first order, the background strain at $r = R_0 + \Delta r$ is $-\partial_r \overline{v}_r \simeq s(1 - 2\Delta r/R_0) = s(1 + 2C)$. Since the background strain is larger, so is the vertical velocity. The reverse is true for the anticyclonic front. The maximum vertical velocities in each solution increase in a nonlinear manner near the time at which the solutions form discontinuities; hence, it is not true that the cyclonic front has the largest vertical velocity at all times (the geostrophic is in fact larger at around $t = 1.8$ days). However, it remains the case that the largest vertical velocity overall occurs for a front curved around a cold core (cyclonic). While the numbers used here are specific to the present example, the qualitative differences are generic.

3. Discussion

Here, we have described the effect of curvature on the dynamics of fronts and eddies, using the idealized configuration of an axisymmetric eddy and associated circular front to simplify the problem. This idealized configuration is the curved analog of the classical, quasi-two-dimensional, infinitely long straight front considered in previous theoretical studies (e.g., Hoskins and Bretherton 1972; Blumen and Wu 1995). Curvature in this system has three direct dynamical effects: (i) The curvature changes the cross-front (radial) force balance from a two-way balance between pressure and Coriolis force—known as geostrophic balance—to a three-way force balance where the pressure and Coriolis forces must combine to provide a net inward centripetal force—known as cyclogeostrophic balance. This changed force balance corresponds to a modified thermal wind equation including the effect of curvature [(6)]. (ii) Curvature modifies the potential vorticity of the system, adding an extra $\partial_z b v_\theta / r$ term to the PV [(3)]. Since PV is conserved in the absence of dissipation, this change to the PV modifies how a given system will adjust to an imposed buoyancy anomaly or large-scale flow. (iii) Curvature also modifies the alongfront (angular) force balance. For an infinitely long straight front, the alongfront force balance states that absolute linear momentum $M = fx + v$ is conserved. For an axisymmetric front/eddy, the alongfront balance instead states that absolute angular momentum $L = fr^2/2 + rv_\theta$ is conserved. In both cases, these conserved quantities allow the definition of conserved cross-frontal coordinates $X = M/f$ and $R = \sqrt{2L/f}$, which are crucial to the formulation of a nonlinear solution for near-discontinuous states. Discontinuities emerge in the solution as a breakdown of the transformation to the conserved coordinate $x \to X$ and $r \to R$ and not as a breakdown of the equations, which remain valid well beyond this point.

The three direct dynamical effects of curvature (effects i, ii, and iii) described above combine to produce significant differences between the adjustment and frontogenesis of a curved front vis á vis that of a straight front as considered by previous theories of adjustment (Blumen and Wu 1995) and frontogenesis (Hoskins and Bretherton 1972). The cyclogeostrophic and geostrophic solutions typically differ by a fraction of order $C \sim v/(rf)$, where v is the geostrophic velocity, r is the radius of curvature, and f is the Coriolis parameter. The effect of curvature is therefore most significant for some combination of sharp frontal gradients, small radii of curvature, and low latitudes where f is small. Where it is significant, curvature has the following major impacts:

- Warm-core (anticyclonic, high PV) axisymmetric eddies have larger, angular velocities for a given PV distribution and are less stable (in the sense they are more likely to collapse or manifest instabilities during an adjustment process) than cold-core (cyclonic, low PV) axisymmetric eddies.
- The alongfront flow for a front curved about a warm (cold) core is stronger (weaker) than for a straight front for the same radial PV profile.
- The vertical velocity associated with frontogenesis forced by a horizontal strain flow is generally stronger for a cyclonic front than a straight front and weaker for an anticyclonic front.
- Anticyclonic fronts sharpen much more rapidly than cyclonic fronts in the same background strain flow (in half the time for the example considered in Fig. 5).

The implication of these results is that cyclonic fronts are likely to be more stable and longer lived in the ocean, and associated with larger vertical tracer fluxes, than their anticyclonic counterparts. This proposed behavior is consistent with observations of the ocean surface layer that show a strong positive bias toward intense cyclonic fronts (e.g., Shcherbina et al. 2013; Rudnick 2001).

There are a number of caveats on the above results. First, we treated both vertical boundaries as rigid surfaces that, while mathematically convenient, do not accurately represent the ocean surface layer. Second, we have limited ourselves to the simplest possible model of a curved front, where the radius of curvature is constant and the front is a perfect circle. While this assumption will never exactly hold, the results will be applicable to a section of smoothly curved front (in the same way that the infinitely long front model is applicable to a section of straight front). However, we acknowledge that perturbations in the azimuthal direction that disrupt the angular symmetry, such as frontal instabilities, can rapidly become a first-order contribution to the flow, at which point the present model becomes invalid. Third, we have assumed that the Coriolis parameter is constant, which makes applying our results at very low latitudes (e.g., to describe tropical instability vortex fronts; Holmes et al. 2014) problematic. Last, we have not considered the large, cross-frontal accelerations associated with time-dependent adjustment and frontogenesis in the presence of large strain rates ($s \sim f$), which for straight fronts have been shown to result in the generation of internal waves (Shakespeare and Taylor 2014) and potentially the collapse of the front during the course of adjustment, preventing the system from reaching the balanced state (Shakespeare and Taylor 2013).

Nonetheless, the theory developed herein provides a robust description of—at the very least—the qualitative impact of curvature on the behavior and stability of density fronts in the ocean.

Acknowledgments. The author thanks Andy Hogg and Ryan Holmes for their comments on an early draft of the manuscript. The motivation for the present paper came from discussions with Ryan Holmes and John Methven over the past several years.

APPENDIX

Nondimensional Equations and the Geostrophic Limit

The model PDE [(16)] may be written in nondimensional form using the scales from (31) as

$$\frac{\partial}{\partial Z'}\left(\frac{R'}{r'}\frac{2C+r'}{C+r'}\frac{\partial C}{\partial Z'}\right)+\frac{\partial}{\partial R'}\left[\frac{q'r'^2}{R'(r'+C)}\frac{\partial C}{\partial R'}\right] =\frac{\partial}{\partial R'}\left(\frac{q'r'}{r'+C}\right), \tag{A1}$$

where

$$r'=-C+\sqrt{C^2+R'^2}. \tag{A2}$$

The nondimensional boundary conditions are

$$\left[R'\left(\frac{2C}{r'}+1\right)\right]\frac{\partial C}{\partial Z'}-\left(\frac{\partial}{\partial R'}q'\right)C=r'\frac{\partial q'}{\partial R'} \quad \text{at} \quad Z'=0, \tag{A3a}$$

$$\frac{\partial C}{\partial Z'}=0 \quad \text{at} \quad Z'=-1, \tag{A3b}$$

$$\int_{-1}^{0}\left(\frac{1}{r'+C}\right)C+\left[\frac{r'^2}{R'(r'+C)}\right]\frac{\partial C}{\partial R'}dZ'=0, \tag{A3c}$$

$$C(R'\to\infty)=0, \quad \text{and} \tag{A3d}$$

$$C=\frac{\partial C}{\partial R'}=0, \quad \text{as} \quad R'\to 0. \tag{A3e}$$

The geostrophic limit is where $R_0\to\infty$ or equivalently $|C|\ll 1$. In this limit the, PDE (A1) becomes

$$\frac{\partial^2 C}{\partial Z'^2}+\frac{\partial}{\partial X'}\left(q'\frac{\partial C}{\partial X'}\right)=\frac{\partial q'}{\partial X'}, \tag{A4}$$

where we define $X\equiv R-R_0$ (or nondimensionally $X'=R'-1$) as the horizontal coordinate relative to the location of the front (R_0). Taking a first-order expansion in C of the coordinate transformation [(A2)] gives $r'=R'-C$ or equivalently $x'=r'-1=X'-C$. Thus, dimensionally, we have that $X=x+v/f$, which is the regular momentum coordinate. The inverse Jacobian of the transformation is

$$J^{-1}=\frac{\partial x}{\partial X}=1-\frac{1}{f}\frac{\partial v}{\partial X}, \tag{A5}$$

which vanishes in the limit of a discontinuity. Equation (A4) is an alternate form of the geostrophic balance equation obtained by previous authors (e.g., Blumen and Wu 1995; Shakespeare and Taylor 2013), here expressed for an arbitrary cross-frontal distribution of PV $q'(X')$. The geostrophic boundary conditions derived from (A3) are

$$\frac{\partial C}{\partial Z'}=\frac{\partial q'}{\partial X'} \quad \text{at} \quad Z=0, \tag{A6a}$$

$$\frac{\partial C}{\partial Z'}=0 \quad \text{at} \quad Z=-1, \tag{A6b}$$

$$\int_{-1}^{0}\frac{\partial C}{\partial X'}dZ'=0, \tag{A6c}$$

$$C(X'\to\infty)=0, \quad \text{and} \tag{A6d}$$

$$C=\frac{\partial C}{\partial X'}=0, \quad \text{as} \quad X'\to -1. \tag{A6e}$$

Note that the left-hand lateral boundary conditions would usually be applied at $X'\to-\infty$, but by our above assumption $X'=X/R_0\ll 1$ and thus applying the boundary condition at $X'=-1$ (as we do herein) is

equivalent for situations where the geostrophic limit is valid. Furthermore, maintaining the same boundary conditions for the geostrophic and cyclogeostrophic models enables a more direct comparison of the dynamics in each case, without the need to consider the effect of different boundary conditions.

REFERENCES

Blumen, W., and R. Wu, 1995: Geostrophic adjustment: Frontogenesis and energy conversion. *J. Phys. Oceanogr.*, **25**, 428–438, doi:10.1175/1520-0485(1995)025<0428:GAFAEC>2.0.CO;2.

Capet, X., J. C. McWilliams, and A. F. Shchepetkin, 2008: Mesoscale to submesoscale transition in the California Current System. Part I: Flow structure, eddy flux, and observational tests. *J. Phys. Oceanogr.*, **38**, 29–43, doi:10.1175/2007JPO3671.1.

Eliassen, A., 1962: On the vertical circulation in frontal zones. *Geofys. Publ.*, **24**, 147–160.

Ferrari, R., 2011: A frontal challenge for climate models. *Science*, **332**, 316–317, doi:10.1126/science.1203632.

Flament, P. J., S. C. Kennan, R. A. Knox, P. P. Niiler, and R. L. Bernstein, 1996: The three-dimensional structure of an upper ocean vortex in the tropical Pacific Ocean. *Nature*, **383**, 610–613, doi:10.1038/383610a0.

Gula, J., M. J. Molemaker, and J. C. McWilliams, 2014: Submesoscale cold filaments in the Gulf Stream. *J. Phys. Oceanogr.*, **44**, 2617–2643, doi:10.1175/JPO-D-14-0029.1.

Holmes, R. M., L. N. Thomas, L. Thompson, and D. Darr, 2014: Potential vorticity dynamics of tropical instability vortices. *J. Phys. Oceanogr.*, **44**, 995–1011, doi:10.1175/JPO-D-13-0157.1.

Holton, J. R., and G. J. Hakim, 2013: *An Introduction to Dynamic Meteorology*. International Geophysics Series, Vol. 88, Academic Press, 532 pp.

Hoskins, B. J., and F. P. Bretherton, 1972: Atmospheric frontogenesis models: Mathematical formulation and solution. *J. Atmos. Sci.*, **29**, 11–37, doi:10.1175/1520-0469(1972)029<0011:AFMMFA>2.0.CO;2.

Liu, M., and T. Rossby, 1993: Observations of the velocity and vorticity structure of Gulf Stream meanders. *J. Phys. Oceanogr.*, **23**, 329–345, doi:10.1175/1520-0485(1993)023<0329:OOTVAV>2.0.CO;2.

Mahadevan, A., 2006: Modelling vertical motion at ocean fronts: Are nonhydrostatic effects relevant at submesoscales? *Ocean Modell.*, **14**, 222–240, doi:10.1016/j.ocemod.2006.05.005.

Niiler, P., N. Maximenko, G. Panteleev, T. Yamagata, and D. Olson, 2003: Near-surface dynamical structure of the Kuroshio extension. *J. Geophys. Res.*, **108**, 3193, doi:10.1029/2002JC001461.

Ou, H. W., 1984: Geostrophic adjustment: A mechanism for frontogenesis. *J. Phys. Oceanogr.*, **14**, 994–1000, doi:10.1175/1520-0485(1984)014<0994:GAAMFF>2.0.CO;2.

Rossby, C. G., 1938: On the mutual adjustment of pressure and velocity distributions in certain simple current systems, II. *J. Mar. Res.*, **1**, 239–263.

Rosso, I., A. M. Hogg, A. E. Kiss, and B. Gayen, 2015: Topographic influence on sub-mesoscale dynamics in the Southern Ocean. *Geophys. Res. Lett.*, **42**, 1139–1147, doi:10.1002/2014GL062720.

Rudnick, D. L., 2001: On the skewness of vorticity in the upper ocean. *Geophys. Res. Lett.*, **28**, 2045–2048, doi:10.1029/2000GL012265.

Sawyer, J. S., 1956: On the vertical circulation at meteorological fronts and its relation to frontogenesis. *Proc. Roy. Soc. London*, **A234**, 346–362, doi:10.1098/rspa.1956.0039.

Shakespeare, C. J., and J. R. Taylor, 2013: A generalized mathematical model of geostrophic adjustment and frontogenesis: Uniform potential vorticity. *J. Fluid Mech.*, **736**, 366–413, doi:10.1017/jfm.2013.526.

——, and ——, 2014: The spontaneous generation of inertia-gravity waves during frontogenesis forced by large strain: Theory. *J. Fluid Mech.*, **757**, 817–853, doi:10.1017/jfm.2014.514.

Shcherbina, A. Y., E. A. D'Asaro, C. M. Lee, J. M. Klymak, M. J. Molemaker, and J. C. McWilliams, 2013: Statistics of vertical vorticity, divergence, and strain in a developed submesoscale turbulence field. *Geophys. Res. Lett.*, **40**, 4706–4711, doi:10.1002/grl.50919.

Tandon, A., and C. Garrett, 1994: Mixed layer restratification due to a horizontal density gradient. *J. Phys. Oceanogr.*, **24**, 1419–1424, doi:10.1175/1520-0485(1994)024<1419:MLRDTA>2.0.CO;2.

Thomas, L. N., A. Tandon, and A. Mahadevan, 2008: Submesoscale processes and dynamics. *Ocean Modeling in an Eddying Regime*, *Geophys. Monogr.*, Vol. 177, Amer. Geophys. Union, 17–38.

Williams, R. T., and J. Plotkin, 1968: Quasi-geostrophic frontogenesis. *J. Atmos. Sci.*, **25**, 201–206, doi:10.1175/1520-0469(1968)025<0201:QGF>2.0.CO;2.